



**FEDERAL UNIVERSITY OF SANTA CATARINA**  
**Undergraduate Course of Materials Engineering**

**Beatriz Cardoso Santos**

**CHARACTERIZATION AND PERFORMANCE EVALUATION OF ABRASIVE  
CUTOFF DISCS**

**Florianópolis**

**2024**

**Beatriz Cardoso Santos**

**CHARACTERIZATION AND PERFORMANCE EVALUATION OF ABRASIVE  
CUTOFF DISCS**

Bachelor Thesis submitted to the Materials Engineering Course at Federal University of Santa Catarina as part of the requirements for obtaining the degree of Materials Engineer.

Supervisor: Dr. Eng. Fernando Moreira Bordin  
Co-supervisor: Prof. Dr. Eng. Fabio Antonio Xavier

**Florianópolis  
2024**

Ficha catalográfica gerada por meio de sistema automatizado gerenciado pela BU/UFSC.  
Dados inseridos pelo próprio autor.

Santos, Beatriz Cardoso  
Characterization and Performance Evaluation of Abrasive  
Cutoff Discs / Beatriz Cardoso Santos ; orientador,  
Fernando Moreira Bordin, coorientador, Fabio Antonio  
Xavier , 2024.  
50 p.

Trabalho de Conclusão de Curso (graduação) -  
Universidade Federal de Santa Catarina, Centro Tecnológico,  
Graduação em Engenharia de Materiais, Florianópolis, 2024.

Inclui referências.

1. Engenharia de Materiais. 2. Disco de corte abrasivo.  
3. Processo cutoff. 4. Usinagem . I. Bordin, Fernando  
Moreira. II. Xavier , Fabio Antonio . III. Universidade  
Federal de Santa Catarina. Graduação em Engenharia de  
Materiais. IV. Título.

**Beatriz Cardoso Santos**

**CHARACTERIZATION AND PERFORMANCE EVALUATION OF ABRASIVE CUTOFF  
DISCS**

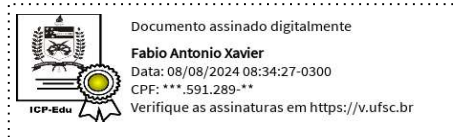
Bachelor Thesis submitted to the Materials Engineering Course at Federal University of Santa Catarina as part of the requirements for obtaining the degree of Materials Engineer.

Florianópolis, 26 de junho de 2024

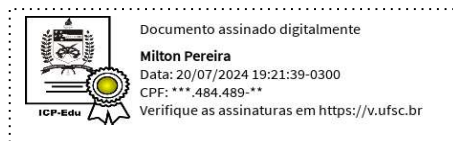


Coordenação do Curso

**Banca examinadora**



Prof. Dr. Eng. Fabio Antonio Xavier



Prof. Dr. Eng. Milton Pereira



M. Eng. Lucas Marra Araujo

Florianópolis, 2024

*“Without the capability to shape and sharpen implements by grinding, we might still be living in the Stone Age.”*

(Stephen Malkin)

## RESUMO

Processos abrasivos, conhecidos por sua alta eficiência e confiabilidade, são fundamentais na manufatura e em diversas áreas na engenharia. No entanto, a interação entre grãos abrasivos, material da peça e o resultado da usinagem ainda é pouco compreendida, tornando essencial a análise detalhada dos discos para otimizar sua produção e desempenho. A fabricação de discos abrasivos é apoiada em centenas de anos de métodos de tentativa e erro, levando à produção customizada das ferramentas à dificuldade de caracterização da estrutura e propriedades intrínsecas. Este processo envolve a seleção criteriosa de grãos abrasivos, mistura de aditivos e uniformidade para garantia de qualidade do produto final. A produção moderna de discos abrasivos tem se beneficiado de avanços tecnológicos, incluindo o controle da microestrutura para personalizar a geometria e distribuição dos grãos abrasivos. Um exemplo dessa técnica é o método de fabricação sol-gel. Esta dissertação investiga o desempenho e as características dos discos abrasivos utilizados em procedimentos de corte, com um foco específico na avaliação de suas propriedades microestruturais, composição de cinzas, coloração de cavacos e experimentos de corte com controle de força. O objetivo principal é reconhecer os atributos que representam eficácia em discos abrasivos. Três discos empregando diferentes abrasivos, óxido de alumínio eletrofundido, óxido de alumínio sol-gel e uma mistura de alumina tenacificada por zircônia (ZTA) e óxido de alumínio, foram examinados e testados com dois materiais de corte, aço inoxidável (AISI 304) e aço baixo carbono com manganês (ST52-3). Por fim, identificou-se o disco de óxido de alumínio sol-gel como a opção preferida devido ao seu método de produção distinto, geometria de abrasivos diferenciada, tamanho de grão maior e volume reduzido de grãos abrasivos. Embora os discos de óxido de alumínio tenham apresentado velocidades de corte mais altas, os discos de zircônia proporcionaram uma longevidade superior. Estudos subsequentes poderiam se concentrar em refinar ainda mais os materiais do disco e os métodos de fabricação para melhorar o desempenho em cenários de corte industrial.

**Palavras-chave:** discos abrasivos; microestrutura; eficiência de corte.

## ABSTRACT

Abrasive processes, known for their high efficiency and reliability, are fundamental in manufacturing and in various fields of engineering. However, the interaction between abrasive grains, workpiece material and the machining result is still relatively unknown, making detailed analysis of the discs essential to optimize their production and performance. The manufacture of abrasive discs is supported by hundreds of years of trial and error methods, leading to the customized production of tools and the difficulty of characterizing the structure and inherent properties. This process involves the careful selection of abrasive grains, additives, and uniformity to guarantee the quality of the final product. Modern abrasive disc production has benefited from technological advances, including microstructure control to customize the geometry and distribution of abrasive grains. An example of this technique is the sol-gel manufacturing method. This dissertation investigates the performance and characteristics of abrasive discs used in cutting procedures, with a specific focus on evaluating their microstructural properties, ash composition, chip coloration and force-controlled cutting experiments. The main objective is to recognize the attributes that make abrasive discs effective. Three discs using different abrasives, electrofused aluminum oxide, solgel aluminum oxide and a mixture of zirconia toughened alumina (ZTA) and aluminum oxide were studied, and tested with two workpiece materials, stainless steel (AISI 304) and low carbon steel with manganese (ST52-3). Finally, the solgel aluminum oxide disc was identified as the top option due to its distinct production method, different abrasives geometry, larger grain size and reduced abrasive grain volume. Although the aluminum oxide discs showed higher cutting speeds, the ZTA discs provided superior longevity. Subsequent studies could focus on further refining disc materials and manufacturing methods to improve performance in industrial cutting scenarios.

**Keywords:** abrasive discs; microstructure; cutting efficiency.

## RESUMO EXPANDIDO

### Introdução

Processos abrasivos, também chamados de usinagem com ferramentas de geometria não definida, são uma tecnologia crítica na engenharia, conhecida por sua alta eficiência e confiabilidade e são aplicados em quase todas as produções, principalmente na manufatura e metalurgia, devido à sua capacidade de moldar, lixar e finalizar materiais. Apesar da disponibilidade de métodos de corte tradicionais, como cisalhamento, torneamento e serragem de metal, o corte com disco abrasivo continua a dominar o cenário industrial. No entanto, a interação entre grãos abrasivos, material da peça e o resultado da usinagem ainda é relativamente desconhecido, então a escolha de um tipo abrasivo apropriado ainda é desafiadora. Uma análise detalhada desses discos torna-se essencial para entender os parâmetros tecnológicos, correlações (força de retificação, temperatura) e resultados do trabalho (desgaste da ferramenta), facilitando a produção de discos otimizados.

### Objetivos

A seleção adequada de discos abrasivos impacta diretamente a produtividade, a eficiência de custos e a qualidade do produto final. Portanto, entender as características de desempenho de diferentes tipos de discos abrasivos em várias condições é essencial para otimizar seu uso.

Este estudo visa analisar as características e o desempenho de três discos abrasivos distintos quando aplicados a duas peças de trabalho diferentes. O disco A tem o abrasivo de óxido de alumínio sol-gel; disco B tem grãos abrasivos de óxido de alumínio; e disco C tem mistura de alumina endurecida por zircônia (ZTA) e grãos abrasivos de óxido de alumínio. As peças de trabalhos utilizadas nos ensaios foram aço inoxidável AISI 304 e aço manganês de baixo carbono ST52-3.

Em resumo, esta investigação explora o comportamento dos discos abrasivos, com o objetivo de otimizar seu desempenho para gerar benefícios econômicos de longo prazo e melhorar a eficiência operacional.

### Metodologia

Na caracterização inicial, amostras menores dos discos foram seccionadas, embutidas em resina epóxi e lixadas com lixas de diamante, seguidas de análise microscópica realizada com um microscópio digital, obtendo-se imagens em duas direções (vista superior e lateral). A tomografia computadorizada de raio-X foi utilizada para analisar a estrutura interna dos discos em 3D, através da reconstrução volumétrica a partir de imagens de projeção adquiridas de diferentes direções. A análise de cinzas foi realizada em duas etapas: inicialmente, a remoção de umidade foi feita colocando os discos em um forno mufla, seguida da queima para geração de cinzas. Após o processo, os grãos abrasivos foram peneirados para determinar seu tamanho, e as cinzas foram analisadas por EDS para identificar os elementos químicos presentes.

Nos experimentos de corte, o primeiro processo envolveu o uso de um rebolo manual para realizar cortes em aço inoxidável AISI 304 e aço carbono ST52-3, com medição da temperatura da superfície durante o corte utilizando um sensor infravermelho. No segundo processo de corte, foi utilizada uma máquina de corte automática com sistema de monitoramento de força em circuito fechado, onde as forças normais aplicadas e as rotações por minuto (rpm) foram predefinidas. Os testes foram



realizados em aço inoxidável AISI 304, com três magnitudes de força (40 N, 32 N e 20 N) e três rotações distintas (6500, 7000 e 8000rpm).

### **Resultados e Discussão**

Na caracterização microestrutural, foi identificado que o disco A apresenta grãos abrasivos em forma de triângulos, indicando um controle meticuloso durante o processo sol-gel, resultando em uma distribuição mais densa. O disco B apresentou grãos de óxido de alumina vermelha, sugerindo a adição de  $\text{Cr}_2\text{O}_3$  para melhorar a dureza, com uma distribuição irregular. O disco C exibiu grãos de duas cores distintas, refletindo a presença de dois tipos de abrasivos. A análise de tomografia computadorizada revelou a taxa volumétrica dos abrasivos dos discos A e B. Para o disco C, a taxa volumétrica não pôde ser calculada devido ao baixo contraste dos grãos de zircônia. No entanto, após o processo de cinzas, foi identificado que o disco C possui o maior volume de abrasivos comparado aos seus concorrentes, enquanto o disco A apresenta a menor quantidade de volume, mas com grãos maiores. O disco B, por sua vez, apresenta o maior volume de poros. Além disso, a análise indicou que o disco A possui dois tipos de materiais aditivos (PAF e criolita), o disco B contém apenas PAF, e o disco C utiliza pirita.

Os resultados do primeiro experimento de corte mostraram que o disco A cortou os materiais mais rapidamente, embora as temperaturas de corte entre os discos não apresentassem diferença significativa, situando-se na faixa de 880°C a 1000°C para todos os discos. O corte com sistema de monitoramento de força em circuito fechado elucidou uma maior taxa de remoção de material e velocidade de corte do disco A, além de menor desgaste da ferramenta e forças de corte reduzidas. O disco C demonstrou maior durabilidade, mas desempenho inferior em termos de velocidade de corte. Já o disco B apresentou maior velocidade que o disco C, porém com menor durabilidade.

### **Considerações Finais**

Com os resultados dos experimentos apresentados, fica claro que o disco A se destaca como a melhor opção para fins de corte abrasivo devido ao seu desempenho excepcional em velocidade de corte, taxa de remoção de material e durabilidade da ferramenta. Apesar dos compromissos envolvidos, sua eficiência e eficácia gerais o estabelecem como um recurso valioso nas atividades de corte industrial.

**Palavras-chave:** discos abrasivos; microestrutura; eficiência de corte.

## LIST OF FIGURES

|  |    |
|--|----|
| <b>Figure 1</b> – Schematic representation of the abrasive cutoff process. ....  | 12 |
| <b>Figure 2</b> – Material removal mechanism in grinding. ....   | 13 |
| <b>Figure 3</b> – Fracture phenomena. A: attritious wear. B: fracture wear. C: grain pullout.<br>.....   | 13 |
| <b>Figure 4</b> – Grain fracture mechanisms. ....  | 14 |
| <b>Figure 5</b> – Comparison of the microstructure and fracture properties of fused (left) and sol-gel aluminum oxide abrasive grains (right).....   | 15 |
| <b>Figure 6</b> – Thermal and mechanical effects influence the material removal mechanisms. ....   | 20 |
| <b>Figure 7</b> – Schematic model for the abrasive cutoff operation. ....  | 21 |
| <b>Figure 8</b> - Photographic images of the (a) abrasive disc; and (b) workpiece. ....  | 23 |
| <b>Figure 9</b> – Experimental setup and expected results flowchart. ....  | 25 |
| <b>Figure 10</b> – Top and side views of the sectioned disc.....   | 26 |
| <b>Figure 11</b> – X-ray Computed Tomography sample of a disc.....   | 27 |
| <b>Figure 12</b> - Schematic image of the cutoff process with temperature measurement control. ....  | 29 |
| <b>Figure 13</b> - Schematic representation of the closed loop force control system.....   | 30 |
| <b>Figure 14</b> – Tool characterization by optical microscopy: Sol-gel aluminum oxide (a). Aluminum oxide (b). Zirconia toughened alumina and aluminum oxide (c).....                         | 31 |
| <b>Figure 15</b> – X-ray computed tomography image analysis: identified abrasive grains with threshold tool (top left). Disconnected particles (bottom left), and 3D volume view (right). .... | 32 |
| <b>Figure 16</b> - XCT image of disc C. Red circle indicates aluminum oxide abrasive grains; yellow circle indicates zirconium oxide abrasive grains. ....                                     | 33 |
| <b>Figure 17</b> – EDS analyzed areas of disc C .....  | 34 |
| <b>Figure 18</b> – Result specter of area 1: ZTA abrasive grain .....  | 34 |
| <b>Figure 19</b> – Result specter of area 2: Al <sub>2</sub> O <sub>3</sub> abrasive grain .....   | 34 |
| <b>Figure 20</b> – Volumetric composition of the discs. ....   | 35 |
| <b>Figure 21</b> – Number of measurements vs temperature: stainless steel workpiece. .   | 36 |
| <b>Figure 22</b> – Number of measurements vs temperature: low carbon steel workpiece.<br>.....   | 37 |
| <b>Figure 23</b> – Sectioned workpieces of stainless (left) and low carbon steel (right). Disc A, B and C indicated in each row.....   | 38 |
| <b>Figure 24</b> – Resulting chip morphology: low carbon (top), and stainless steel chips (bottom); for discs A, B and C. ....   | 38 |
| <b>Figure 25</b> – Force control cutting test results: 40N force. ....   | 39 |
| <b>Figure 26</b> – Force control cutting test results: 32N force.....  | 40 |
| <b>Figure 27</b> – Force control cutting test results: 20N force.....  | 40 |

## LIST OF CONTENTS

|          |   |           |
|----------|---|-----------|
| <b>1</b> | <b>INTRODUCTION.....</b>                | <b>9</b>  |
| <b>2</b> | <b>LITERATURE REVIEW .....</b>          | <b>11</b> |
| 2.1      | ABRASIVE CUTOFF PROCESSES .....         | 11        |
| 2.2      | ABRASIVE CUTOFF DISC .....              | 15        |
| 2.3      | CHARACTERIZATION OF ABRASIVE TOOLS..... | 18        |
| 2.4      | GRINDING HEAT.....                      | 19        |
| <b>3</b> | <b>EXPERIMENTAL METODOLOGY.....</b>     | <b>23</b> |
| 3.1      | MICROSTRUCTURE CHARACTERIZATION.....    | 25        |
| 3.2      | X-RAY COMPUTED TOMOGRAPHY (XCT) .....   | 26        |
| 3.3      | ASH ANALYSIS .....                      | 27        |
| 3.4      | TEMPERATURE EXPERIMENTS .....           | 28        |
| 3.5      | FORCE CONTROL CUTTING EXPERIMENTS.....  | 29        |
| <b>4</b> | <b>RESULTS.....</b>                     | <b>31</b> |
| 4.1      | TOOL CHARACTERIZATION .....             | 31        |
| 4.2      | X-RAY COMPUTED TOMOGRAPHY (XCT) .....   | 32        |
| 4.3      | ASH ANALYSIS .....                      | 33        |
| 4.4      | TEMPERATURE EXPERIMENTS .....           | 36        |
| 4.5      | FORCE CONTROL CUTTING EXPERIMENT .....  | 39        |
| <b>5</b> | <b>CONCLUSION.....</b>                  | <b>42</b> |
|          | <b>REFERENCES .....</b>                 | <b>44</b> |

## 1 INTRODUCTION

Abrasive processes, also called machining with geometrically undefined cutting edges, are a critical technology in engineering, known for its high efficiency and reliability. But to this day, the design of machining processes is still largely empirical. (KLOCKE, 2009). They are applied in nearly every production, and are also core technologies in developing new energy systems as well as in improving efficiency of existing products. However, the interaction between abrasive grains, workpiece material, and the machining result is still relatively unknown (LINKE, 2016).

The formulations of abrasive tools and the methods used for their production are predominantly proprietary to companies. As the design process of a grinding tool relies on the expertise of the manufacturer; it is often not a transparent procedure to the customer (LINKE, 2016). In industrial settings, the use of abrasive discs for steel cutting remains prevalent owing to its efficiency and economic advantages. Despite the availability of traditional cutting methods such as turning, and metal sawing, abrasive disc cutting continues to dominate the industrial landscape. This study explores the behavior of abrasive discs, with the aim of optimizing their performance to yield long-term economic benefits and enhance operational efficiency.

This study explores the behavior of abrasive discs to optimize their performance, aiming to achieve long-term economic benefits and enhance operational efficiency. Abrasive discs play a crucial role in providing controlled material removal and are commonly employed in electric tools such as sanders and grinders. A detailed analysis of these discs becomes essential to understand the technological parameters, correlations (grinding force, temperature), and work results (tool wear), facilitating the production of optimized discs. Such optimization not only leads to financial savings but also significantly boosts material removal rates, thereby reducing task completion times and improving operational efficiency.

Various experiments can be conducted to characterize abrasive processes. Surface roughness measurements can show the quality of finished surfaces, while material removal rate testing evaluates efficiency. Analysis using energy-dispersive X-ray spectroscopy (EDS) examines the chemical composition of the abrasive tools. Thermal analysis with embedded thermocouples provides data on the grinding processes thermal impact. Through a systematic examination and comparison of

various abrasives and their impact on the final product, this research attempt to evaluate discs available in the market and delineate the characteristics indicative of superior efficiency. The study employs three distinct types of abrasive discs and utilizes two different material workpieces.

A critical element of the methodology involves a force control cutting test, conducted to assess wear between abrasive discs using a bench machine, designed to simulate the manual cutting process. The results encompass data related to mechanical forces (normal force and torque), wear, required mechanical power, and rotation, offering insights into the performance of different discs under varying conditions.

Furthermore, optical microscopy, x-ray computerized tomography (XCT) and ash analysis examinations of different discs are conducted to gain deeper insights into the tools used. These analyses lay a foundation for subsequent comparisons between the tools, facilitating the exploration of the characteristics of the discs and contributing to a comprehensive analysis of abrasive cutting.

Additionally, another cutting test was performed, this time monitoring temperature during the grinding process using an infrared thermometer. This allows analysis of the heat radiation emitted and reflected by the object, converting these data into temperature values, and providing an analysis of thermal dynamics during abrasive grinding.

In summary, this investigation aims to understand the characteristics of the discs available on the market and exam the influence of grinding on workpiece and cutting results. The methodology, coupled with the specificity of the chosen abrasives and materials, is poised to make a contribution to the field of abrasive processes.

## 2 LITERATURE REVIEW

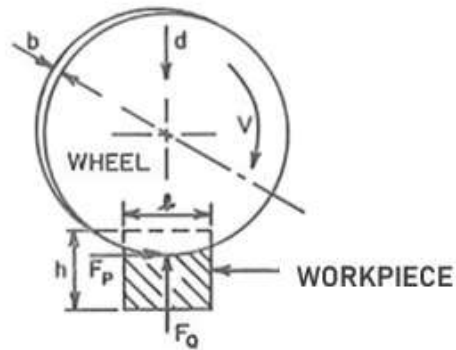
### 2.1 ABRASIVE CUTOFF PROCESSES

Grinding, a highly intricate mechanical method of abrasive machining, is designed to process hard or brittle materials by leveraging abrasive particles that are substantially harder than the material being machined. The abrasive particles, possessing irregular shapes and oriented edges, and are bound together by bonds (MACHADO *et al.*, 2009). These bonds play a pivotal role in shaping the abrasive processes, providing the structural integrity necessary for efficient material removal. The tools used in grinding operations can be made from a variety of abrasives, from traditional materials like aluminum oxide and silicon carbide to advanced super abrasives such as cubic boron nitride (CBN) and synthetic diamond. The selection of these abrasives depends on the specific material characteristics and desired outcomes of the grinding process. The abrasive processes encompass all production methods where hard abrasive grits are employed for material removal, whether it be for initial shaping, final touches, or large-scale material removal. The control of all parameters requires context knowledge in order to accomplish the intended outcomes (KUFFA, 2017).

Metal grinding is classified as a machining process, involving the mechanisms of material removal through a process of forming chips. Unlike other cutting methods that use a tool with a known geometry and orientation, grinding uses many abrasive grains with different shapes (MALKIN, 1968). As the tool rotates, the abrasive grains remove material in the form of chip. These resistant abrasive grains are identified as a cutting tool with an undefined geometry and are held together by a bonding resin to create a grinding disc. Notably, these operations are often carried out in a dry environment, free of lubricating fluids, relying solely on the abrasive power of the wheels in the ambient air. The operational approach typically involves the radial movement of the wheel through the workpiece (radial feed rate  $v_{fr}$ ), a procedure that demands careful consideration of numerous factors to ensure optimal outcomes. The contact length ( $l$ ) between the wheel and workpiece (see Figure 1) is a critical variable as it significantly impacts whether there is ample space between the abrasive grains to accommodate the generated chips. Insufficient space can lead to excessive wheel

wear or loading. Cutting forces are also important as they affect the mean force per grain and the surface temperature of the wheel. (SHAW, FARMER and NAKAYAMA, 1967).

**Figure 1** – Schematic representation of the abrasive cutoff process.



Source: Shaw *et al.* (1967).

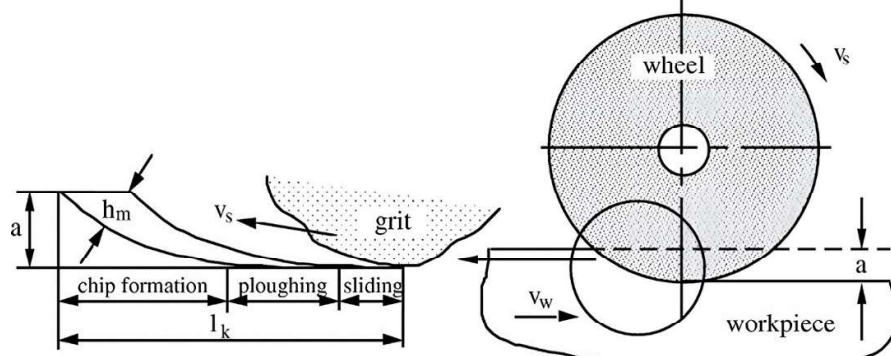
In essence, the world of metal grinding unfolds as an interplay of abrasive grains, grinding wheels, and workpieces, where the intricate control of variables ensures not only the efficiency of material removal but also the longevity and effectiveness of the grinding tools involved. The continuous evolution and refinement of these processes contribute to the advancement of metalworking techniques, embodying the balance between precision and pragmatism.

Hahn (1962 *apud* CARREIRA, 2022, p. 17) proposed a model that describes the interaction between grain and workpiece in plane grinding, as shown in Figure 2. The working penetration is represented by letter  $a$ ,  $hm$  is the maximum chip thickness and  $lk$  is the cutting path length. In this case, chip removal is divided into three phases: in the first phase, the grain slides over the surface without cutting, only causing elastic deformation; in the second phase, known as ploughing, with the increase in stress at the grain/workpiece interface, the elastic regime is broken and plastic deformation occurs; finally, the chip is formed when the accumulated material can no longer withstand the shear stresses and is removed from the matrix.

Hahn's model not only serves as a theoretical framework but also offers a practical lens through which the complexities of plane grinding can be interpreted. The interplay of parameters, phases, and outcomes described by this model forms a foundation for refining and advancing metal grinding techniques, contributing to the

continual evolution of machining processes in the realm of material science and engineering.

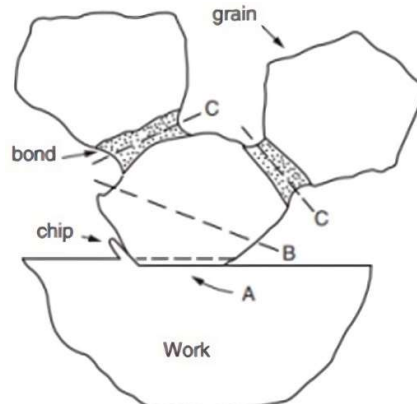
**Figure 2** – Material removal mechanism in grinding.



Source: Carreira (2022).

To effectively manage tools and maintain the operational efficiency of grinding processes, a detailed understanding of wear mechanisms is required. Wear is a combination of physical separation, chemical dissolution, and melting. Malkin (2008) illustrates the complex mechanisms that underlie this type of wear, which are evident through three main avenues (see Figure 3): fracture of the abrasive grains, wear due to abrasion, and fracture of the bond. The fracture wear, greatly influenced by its friability, involves a portion of the grain breaking off, subsequently creating a new cutting edge. Simultaneously, the attritious wear causes the edges to gradually become rounded, which has a negative impact on both the cutting efficiency and the final quality of the machined surface. With the large increase in mechanical stresses, the abrasive is unable to efficiently remove material and reaches a critical threshold, causing the bond structure to fracture in individual abrasive grits (grain pullout).

**Figure 3** – Fracture phenomena. A: attritious wear. B: fracture wear. C: grain pullout.

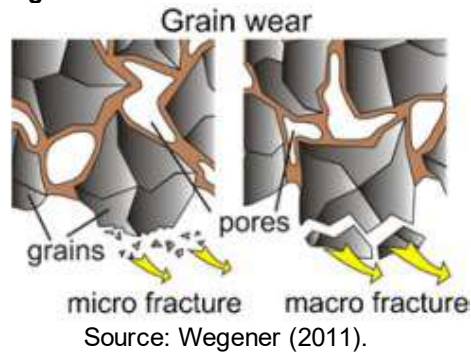


Source: Malkin (2008).



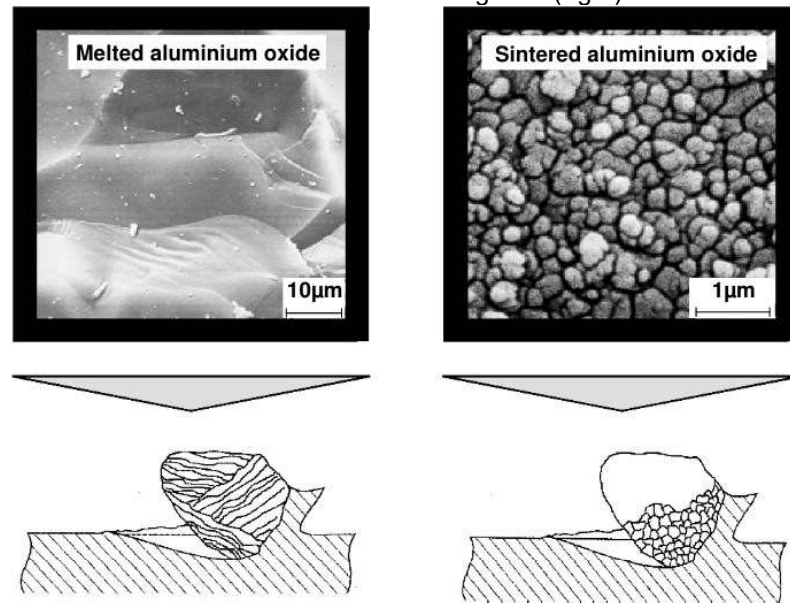
The breakage of aluminum oxide abrasive grains can occur in two separate ways: electrofused grains tend to suffer macro fracture, while sol-gel grains present a microcrystalline fracture, as illustrated in Figure 4. A study conducted by Starkov et al. (2014), corroborated by Naldony (2014), showed that when the abrasive with a microcrystalline structure fracture, the breakage occurs in smaller and more uniform fragments due to the sintering process of the microcrystalline abrasives during manufacturing, which prompts an intragranular breakage along the sintering boundaries, instead of the cleavage plane breakage absorbed in polycrystalline/monocrystalline aluminum oxides.

**Figure 4 – Grain fracture mechanisms.**



As cited by Klocke (2009), the microcrystalline structures found in the sol-gel aluminum oxide abrasive grains, has dislocation yield stress at grain boundaries, enhancing toughness and resulting in a favorable fracture behavior when compared with fused corundum. As is possible to see on Figure 5, only small particles chip off and the grit maintains its sharpness.

**Figure 5** – Comparison of the microstructure and fracture properties of fused (left) and sol-gel aluminum oxide abrasive grains (right)



Source: Klocke (2009).

In a sense, abrasive grit wear is a continuous process, shifting from micro-wear (focus solely on the abrasive) to macro-wear, in which there is a reduction of the cutting tool dimensions by bond fracture and consequently abrasive grain pullout, as well as corner wear.

## 2.2 ABRASIVE CUTOFF DISC

The complete abrasive grinding disc is made of abrasive particles, resin bond, fillers, fiber mesh, and a metal ring. At the core of this composite structure are abrasive ceramics grains, distinguished by their fundamental attribute of hardness or wear resistance. A requisite level of toughness is indispensable to prevent easy fracture of these abrasive particles, a critical factor in sustaining their effectiveness over prolonged usage. Furthermore, acknowledging the potential generation of elevated temperatures due to abrasive friction, a refractory feature within the abrasive particles is essential, aligning with the insights provided by Callister (2016). The selection of the abrasive material is crucial to ensure the effectiveness of the cutting process. Choosing the right abrasive grain allows for efficient material removal rates, which reduces the time and effort required to complete the cutting process.

Aluminum oxide, also known as corundum, stands out as one of the most efficient abrasive materials available. Aluminum oxide grains are produced in pot type electric-arc furnaces, with the calcination of the raw material, bauxite, at approximately 950°C to remove moisture. Following this, ground coke and iron borings are mixed with the calcined bauxite. An electric current generates intense heat, around 2000°C, causing bauxite to melt and impurities to settle at the bottom of the furnace. Additional bauxite mixture is continually added until the furnace reaches capacity. Upon emptying the furnace, the outer impurities are stripped away, leaving behind aluminum oxide, which is then processed into abrasive grains (BHOWMIK and NAIK, 2018). Due to its exceptional hardness and durability, corundum keeps a sharp cutting edge and resists deformation during abrasive operations (KLOCKE, 2009). Its prolonged durability reduces the need for frequent replacements, resulting in cost savings and guaranteeing the integrity of the disc during use, which significantly reduces the risk of accidents. In this research, the aluminum oxide grains studied can be electrofused or sol-gel.

The sol-gel method involves preparing a sol, a stable colloidal suspension of nanoscale particles. Through hydrolysis and condensation reactions, the sol is transformed into a three-dimensional gel of suspended nanoparticles. The sol-gel method offers advantages such as control over the grain size, composition, and purity of the particles.

Zirconia toughened alumina (ZTA), or also called specialized alumina or Zirconia Aluminum Oxide, have a combination of two materials, and so, features unique characteristics. Zirconia, known for its strength and resistance to heat, when combined with alumina, creates a synergy that improves abrasive properties. Based on studies on dynamic fatigue and wear resistance have demonstrated that stress-induced transformation improves the static fatigue properties. Nevertheless, the wear resistance of zirconia toughened alumina decreased in comparison to pure alumina, which was linked to the presence of microcracks on the surface caused by stress induced transformation. (WANG and STEVENS, 1989).

Resin bonds, typically composed of phenolic resin, a thermosetting polymer, play a pivotal role in cohesive combination, constantly holding the abrasive particles together. This particular category of resin experiences an irreversible process of solidification during the formation of a network, thus maintaining its structural integrity

even when subjected to elevated temperatures. The inherent rigidity, durability, and dimensional stability of thermosetting polymers, when compared to thermoplastics, contribute significantly to the overall strength of the bonds formed by the resin (CALLISTER, 2016). Due to its strong thermal stability of the thermosetting resins used in the disc's formulation, abrasives can withstand elevated temperatures without degrading their qualities. This property guarantees the integrity and lifespan of the abrasive material and helps prevent premature deterioration of the matrix. The high heat resistance of the resin helps to extend the life of the disc and maintain consistent performance, even during grinding in elevated temperature conditions (KLOCKE, 2009).

Recognizing the inherent fragility of these resin bonds, reinforcements become essential in order to enhance the safety and longevity of the process of material removal, a principle supported by Linke (2016). Consequently, cut-off wheels are strategically reinforced with materials such as glass fibers, nylon discs, and other agents that enhance strength, as emphasized by Colleselli (1988). The specific patterns in which the fibers are joined introduce variations in the types of weaves or interlaces, thereby impacting the extension characteristics and overall performance attributes of the reinforcing body. (LINKE, 2016).

An additional pivotal element in the composition of the grinding disc is the strategic use of fillers, employed to modify the properties of resin systems. Fillers help adhere the grain to the bond, increasing the mechanical strength of the disc. Prevent thermal degradation of the resin, cool the tool while it is operating and much more. (RUDAWSKA, 2018). In the form of solid lubricants, fillers can reduce friction at the wheel-workpiece interface and preserved sharpness of the abrasive grits. (LINKE, 2016). The selection of fillers involves nuanced considerations, including cost, density, resin absorption by the filler, filler loading, and particle size distribution. The insights presented by Laza *et al.* (2007) stress the need for meticulous consideration of the curing process and the intended use of the final composite, signifying the importance of optimal filler selection for achieving desired material properties.

Cryolite (sodium aluminum fluoride) is a filler that melts at elevated temperatures, causing increased porosity and enhancing the grinding process effectively (KNOP and PILATO, 1985). Acting as a grinding aid with lubricating characteristics, this compound has the potential to enhance overall performance

(COES, 1955). Sulfur-containing additives, such as pyrite (iron sulfide), are utilized to retard the creation of strongly adherent metal oxide layers through an oxidation-reduction reaction at elevated temperatures. These additives also slow down the oxidative deterioration of phenolic resin bonding, extending the lifespan of the wheel. Potassium aluminum fluoride (PAF) serves as a filler and a binder, effectively attaching the abrasive to the abrasive surface. The binder material must have adequate bond strength to prevent the abrasive from pulling. Simultaneously, it should exhibit sufficient toughness to withstand the axial and radial forces generated during the grinding operation. Furthermore, PAF can rapidly dissipate the generated heat from the workpiece to maintain a cool temperature, consequently preventing oxidation. The chemical interaction between PAF and the workpiece surface enhances the abrasive efficiency of the process.

In summary, the interplay of abrasive particles, resin bond, and fillers in an abrasive grinding disc represents an intricate engineering undertaking. This comprehensive understanding not only elucidates the complexities of material removal processes but also emphasizes the continual evolution and refinement of abrasive technology in the realm of engineering and manufacturing.

### 2.3 CHARACTERIZATION OF ABRASIVE TOOLS

The characterization of abrasive cutting discs in the literature focuses on various parameters that influence cutting performance and disc wear. For instance, Ortega (2020) conducted study using the following methods: measuring weight loss, analyzing disc profile and surface topography, and digitizing disc surfaces to evaluate cutting ability and surface roughness. Techniques such as optical microscopy, confocal microscopy, portable profilometry, scanning electron microscopy, and computerized tomography were employed to gain insights into disc structure and wear patterns.

Goldstein *et al.* (2003) used energy dispersive X-ray spectroscopy (EDX) with scanning electron microscopy (SEM) for detailed elemental analysis of abrasive grains and binders. The combination of these techniques allowed for precise characterization of the chemical and microstructural compositions of the abrasive materials.

Malkin and Guo (2008) described test methods for wear and durability of abrasive discs, addressing simulations of real cutting conditions. Their work was

essential to understanding the efficiency and service life of discs, influencing the design of more durable abrasive tools.

Bianchi *et al.* (2006) examined the impact of binder hardness on cutting force and the grinding ratio. They used abrasive discs with three different hardness levels and observed a slight increase in cutting force with increased hardness. However, there were no significant differences in the G-ratio. Neugebauer *et al.* (2005) analyzed the influence of the shape of Al<sub>2</sub>O<sub>3</sub> abrasive particles on the number of cuts per disc. They investigated three types of grain geometries in cutting tubes of different materials and diameters.

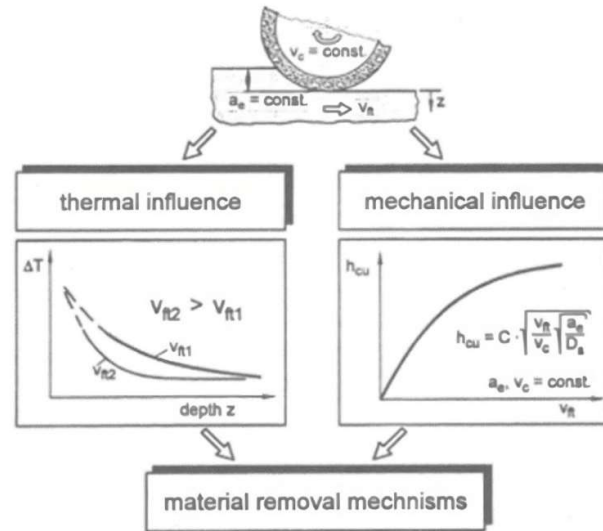
Bordin *et al.* (2021) characterized through X-ray computed tomography the abrasive, pore and bond content of conventional aluminum oxide grinding wheels, with mixtures of electrofused and sol-gel abrasive grits. The authors were able to discern that, even with the same label description, the grinding wheels showcased different volumetric content.

The most influential variables of grinding are the type and size of the abrasive grit. In contrast, disc cost and tool life are crucial aspects in the daily production work. Thereby, the characterization methods used in this research aim to consider all these variables to evaluate the performance of the studied discs.

## 2.4 GRINDING HEAT

The central outcomes of any material removal process revolve around the significant thermal and mechanical effects, prominently illustrated in Figure 6. This graphical representation provides a clear depiction of how these effects play a crucial role in shaping both the material removal process and the integrity of the resulting surface. In essence, the intricate relationship between thermal and mechanical impacts is linked, shaping the overall performance and quality of the material removal process. The comprehensive understanding of these intertwined mechanisms, as emphasized by Marinescu *et al.* (2015), underscores the complexity inherent in this process, highlighting the challenge of disentangling their distinct impacts on material removal mechanisms and surface integrity.

**Figure 6** – Thermal and mechanical effects influence the material removal mechanisms.

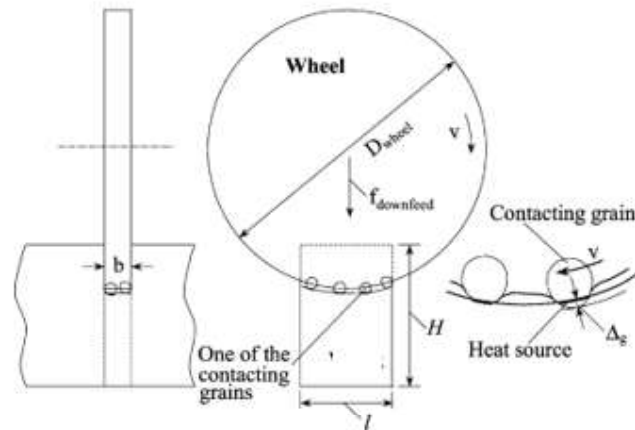


Source: Marinescu *et al.* (2015).

The grinding process is characterized by a significant energy consumption per unit volume of material removed. Nearly all of this energy is transformed into heat, which becomes concentrated within the grinding area. The elevated temperatures generated during grinding have the potential to induce a diverse form of thermal effects on the workpiece, including burning, alterations in phase, tempering of the surface layer, potential subsequent hardening, detrimental residual tensile stresses, the development of fractures, and a reduction in strength against fatigue (MALKIN and GUO, 2008). The chosen abrasive, bond, grain size and grain concentration will determine the thermal and mechanical tool quality.

As per Hou and Komaduri (2004), the distribution of heat among the chip, workpiece, and abrasive grains was systematically explored using the grain-workpiece interface heat source model (see Figure 7). The findings from this study revealed, contrary to the grinding process with vitreous conventional grinding wheels, a substantial allocation of heat, ranging from 60% to 75%, directed into the chip, approximately 20% to 35% into the workpiece, and only a minimal fraction into the abrasive grains. This distribution aligns with the inherent nature of cut-off operations, which bear resemblance to cutting processes but involve the utilization of high negative rake tools.

**Figure 7** – Schematic model for the abrasive cutoff operation.



Source: Hou and Komaduri (2004).

The intricate interplay of energy conversion and heat distribution elucidated by these studies emphasizes the multifaceted nature of thermal effects in the grinding process. As a result, a comprehensive understanding of these thermal dynamics is crucial for optimizing the selection of abrasive tools and minimizing the potential for adverse thermal consequences on the workpiece. The complexity disclosed in the distribution of heat provides valuable insights for refining and enhancing the efficiency of grinding operations, contributing to advancements in the field of material removal processes.

One possible effect of heat during dry grinding is the appearance of temper colors on the workpiece and chip. Tempering is a common heat treatment for steels, and temper colors are the discoloration that occurs when steel is heated at high temperatures. The colors are created by light interference in thin layers, where oxygen from the air causes an oxide layer to form, resulting in a temperature-specific color. The thickness of the oxide layer depends on the diffusion depth of the oxygen atoms, which is temperature dependent. (CALLISTER, 2016).

According to Ning, Rahman and Wong (2001), the higher the cutting speed and feed rate, the darker the color of the chip and the greater the degree of oxidation, which leads to a higher temperature. The colors identified in his experiment are shown in Table 1.



**Table 1** – Temper color and temperature of the chip.

| <b>Temper color</b> | <b>Chip temperature [°C]</b> |
|---------------------|------------------------------|
| Dark blue + green   | >1000                        |
| Dark blue           | 960 - 1000                   |
| Dark blue + purple  | 920 - 960                    |
| Golden brown        | 820 - 860                    |
| Yellow              | 800 - 840                    |

Source: Ning (2001).

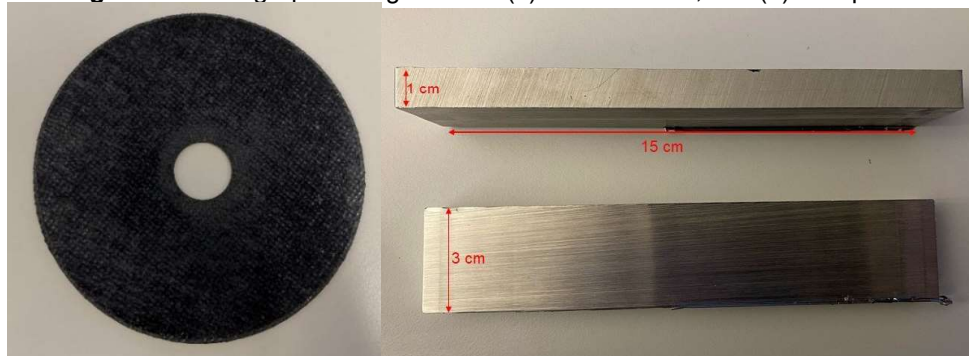
### 3 EXPERIMENTAL METODOLOGY

The experimental procedure involves the utilization of three abrasive discs applied to two distinct workpieces composed of varied materials. For confidentiality reason, the disc brands must be omitted, so the identification will be by letter and characteristic:

- Disc A has sol-gel aluminum oxide abrasive material,
- Disc B has aluminum oxide abrasive grains, and
- Disc C has a mixture of zirconium toughened alumina (ZTA) and aluminum oxide abrasive grains.

All the three discs analyzed (Figure 8a) in this study have the same dimensions: outer diameter and width, equal to 125mm and 1mm, respectively. The initial workpiece dimensions were 10mm x 15mm x 30mm as highlighted in Figure 8b.

**Figure 8** - Photographic images of the (a) abrasive disc; and (b) workpiece.



Source: The author (2024).

The selection of these discs is based on their specific material characteristics, which will provide valuable insights into the material removal process. Disc A (A60SBF41) is known for its cutting efficiency and durability, making it ideal for general metalworking applications such as ferrous metals, stainless steel, steel alloys, and gray cast iron. Disc B (A60TBF41) offers simplicity and accessibility compared to Disc A, which has higher added value. It is recommended for routine metal cutting, including the cutting of steel rebar, angle profiles, tubes, and sheets. Disc C (Z60VBF41) adds complexity with its zirconia composition, known for its toughness and heat resistance. It is designed for cutting metals in the form of rods, gutters, angle profiles, tubes, and sheets. Especially developed for cutting steel and stainless steel.

An important choice in this study is the selection of resin-bonded abrasive discs. These wheels represent a specific grinding process in which the focus is on the cut, rather than on the final surface and topography of the workpiece. In this process, the grinding disc must remain sharp and does not undergo a dressing process. Thus, a resin matrix allows the disposal of "used" grains, continuously presenting new grains and maintaining sufficient strength to hold the grains while they are still active.

The two workpiece bars used in this study are composed of materials representing real-world applications, stainless steel AISI 304 and ST52-3, a low carbon manganese steel. Table 2 and Table 3 show the chemical compositions of each steel.

**Table 2** – Chemical composition of the AISI 304 stainless steel.

| <b>Carbon</b> | <b>Silicon</b> | <b>Manganese</b> | <b>Phospor</b> | <b>Sulphur</b> | <b>Chromium</b>  | <b>Nickel</b>   | <b>Nitrogen</b> |
|---------------|----------------|------------------|----------------|----------------|------------------|-----------------|-----------------|
| 0.07 %        | 1.00%          | 2.00%            | 0.45%          | 0.0015%        | 17.5 –<br>19.5 % | 8.0 –<br>10.5 % | 0.10 %          |

Source: HABA Solutions in Plates. Technical specification of Inox V2A.

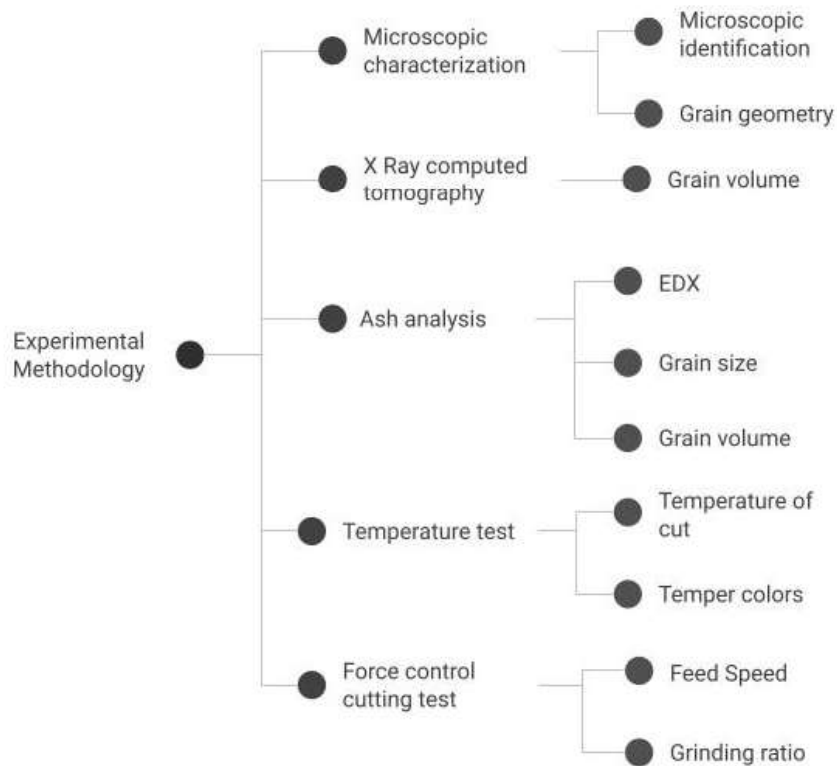
**Table 3** – Chemical composition of the ST52-3 low carbon steel.

| <b>Carbon</b> | <b>Silicon</b> | <b>Manganese</b> | <b>Phosphor</b> | <b>Sulphur</b> |
|---------------|----------------|------------------|-----------------|----------------|
| 0.20 %        | 0.55 %         | 1.60 %           | 0.035 %         | 0.035 %        |

Source: HABA Solutions in Plates. Technical specification of Konstrukta 52.

This selection serves to introduce variability into the experimental setup, enabling a comprehensive assessment of the abrasive disc's performance across diverse material compositions, allied to the abrasive disc structure and composition characterization, leads to broader point of view in terms of abrasive disc analysis. Figure 9 is a flowchart illustrating the experimental setup and its corresponding expected outcomes.

**Figure 9** – Experimental setup and expected results flowchart.



Source: The author (2024).

### 3.1 MICROSTRUCTURE CHARACTERIZATION

The initial characterization of the tools involved optical microscopy. For the microscopy analysis to be possible, it was necessary to section two smaller segments of each disc, embed them and sand the resin coat and fiberglass, so the abrasive grains can be evaluated.

The smaller samples were taken from the discs by a Struers cutoff machine Lobotom-5. A diamond wheel was employed to section the samples. These smaller specimens were dipped in a highly transparent two-component cold mounting material, epoxy resin QPREP KEM 92, with a mixture of 50g of resin for 11.5g of hardener. Poured in a mounting mold with the sample. The molding process uses a vacuum infiltration and pressure device for 20 minutes. These cold embedding materials must be cured in a pressure device under positive pressure (2 - 2.5 bar). This increases the boiling point of the embedding material and suppresses the formation of gas bubbles

during polymerization. After the cure time of 24 hours, the solidified resin was ready to be prepared.

The sanding was performed with diamond sandpapers to access the interior of the disc, and not only its surface. Since the samples had abrasive grains, a normal sandpaper of aluminum oxide was not going to be enough. Consequently, the sample was manipulated with 3 different granulometry (220, 500 and 1200 mesh), for 15min with 40N and 300 $\mu$ /min in a grinding and polishing machine Saphir 550 with Rubin 520 head for working wheels. After sanding, the specimen was taken to an ultrasound bath for 5 minutes and submitted to a drying process by an air jet to avoid corrosion.

All the microscope analyses were made in the Keyence digital Microscope VHX – 700. For the embedded samples, two directional pictures were taken of each disc. A picture of the top view of the sectioned disc, to have a transversal view of the interior of the disc; the second picture should be a side picture of the sectioned disc, to obtain the profile of the interior of the disc, as illustrated in Figure 10. Each of these directional pictures were taken with a magnification of 20, 50 and 100 times.

**Figure 10** – Top and side views of the sectioned disc.



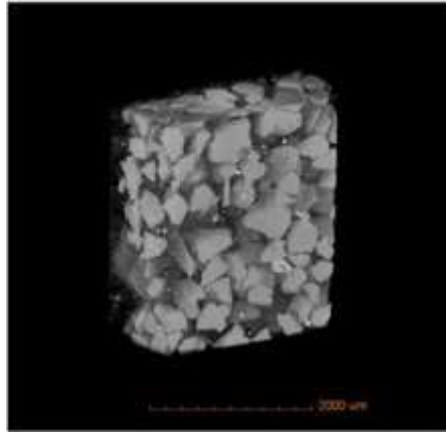
Source: The author, 2023.

### 3.2 X-RAY COMPUTED TOMOGRAPHY (XCT)

X-ray computed tomography is a technology to analyze structures in three dimensions where projection images of a specimen acquired from different directions are used to reconstruct its volumetric representation (LEIßNER *et al.*, 2019). The computed tomography was performed externally to the Inspire AG laboratory, in the Porous Media and Thermophysical Properties Laboratory. (LMPT/ UFSC). The sample

used in the XCT is exemplified in Figure 11, and the resultant images were sent for review.

**Figure 11** – X-ray Computed Tomography sample of a disc.



Source: LMPT (2023).

The image analysis was conducted using Fiji /ImageJ software, and the process to treat the data involved importing the images into the software, correcting brightness, and contrast, identifying abrasive grains using the Threshold tool, and disconnecting particles for 3D volume analysis. The analysis further includes the determination of particle size distribution and the computation of the volume rate. The results provided a detailed 3D image representation of the sample, offering valuable insights into its internal structure and characteristics. This analytical approach can be used for diverse applications, contributing to a better understanding of materials through comprehensive image analysis.

### 3.3 ASH ANALYSIS

Ash analysis is part of the reverse engineering process used to identify as much information as possible about the discs chosen for this research, mainly: bonding material, filler material, size, volume, weight, and composition of the abrasive grains. This portion of the study is divided into two distinct steps. The initial step is focused on eliminating the moisture from the samples. To achieve this, the discs were placed in the Thermo Scientific™ Heratherm™ Advanced Protocol Ovens at 110°C for a duration of 8 hours.

Following the drying process of the discs, it becomes necessary to conduct various measurements. These measurements include assessing the removed humidity, determining the weight of the metal disc, and recording the weight of the disc after its initial exposure to the oven.

The next step involves the ash process itself. During this phase, the discs, excluding the metal ring, must be positioned inside a ceramic crucible. These crucibles are then placed in an ash furnace; this time, they remain heated for a period of 12 hours at a temperature of 550°C. This step is crucial to evaporate the resin content, leaving only the fiber, abrasive grains, and ash in the crucible. After the process, the mesh must be removed, and the ash and abrasive grains are saved and analyzed separately.

The abrasive grains extracted from each disc posterior the ash process go through sieving with various mesh sizes to determine their size. Meanwhile, the ashes are analyzed using EDX, where the elements present in them are identified, helping to discern the type of filler used in each disc.

### 3.4 TEMPERATURE EXPERIMENTS

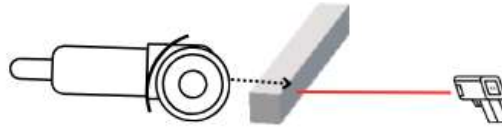
To guarantee the optimal state of the abrasive discs for experimentation, the same procedure utilized in the ash analysis to eradicate any trace of humidity was performed, the discs are subjected to a controlled temperature of 110 °C for an extended duration of 8 hours in a muffle furnace.

In the temperature experiments, each individual disc is attached to a manual angle grinder, a bar measuring 10mm x 30mm x 150mm serves as the workpiece for the abrasive trials. Within the experimental framework, a total of 5 cuts are systematically executed on the bar, providing a comprehensive evaluation of the abrasive disc performance.

The advanced Voltcraft IR2201-50D USB IR-Thermometer, an infrared laser gun, serves as the measuring instrument in this experimental setup. Its function is to gauge the surface temperature of the materials subjected to the abrasive cutting process. Operating on the principles of infrared thermometry, this device utilizes a sensitive sensor to analyze the heat radiation emitted and reflected by the object under examination. To avoid imprecise measuring values, emissivity levels can be set.

During the grinding operation, the infrared laser gun is strategically positioned at a 90° angle at the end of the bar, as depicted in Figure 12. This positioning ensures optimal coverage and a thorough assessment of the thermal changes occurring at the cutting interface. To initiate the temperature measurement, the measuring button is pressed, activating the permanent measurement function. This feature allows the thermometer to continuously record temperature data until the measuring button is pressed again, ensuring comprehensive and uninterrupted monitoring of the thermal profile throughout the grinding process.

**Figure 12** - Schematic image of the cutoff process with temperature measurement control.



Source: The author (2014).

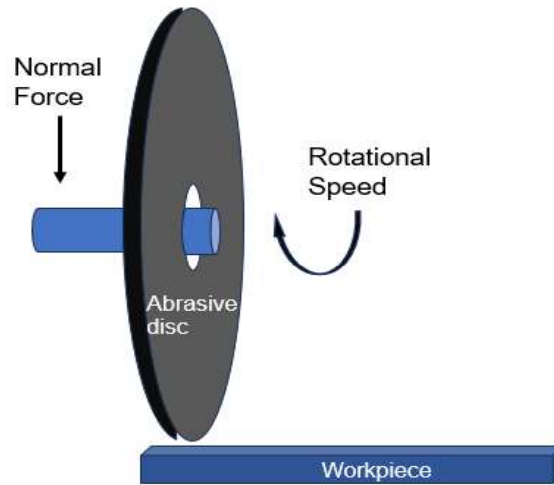
As the abrasive disc progresses through the material, it generates heat through its mechanical action, a phenomenon intricately captured by the infrared laser gun. During each cut, the thermometer takes a reading of the bar temperature.

### 3.5 FORCE CONTROL CUTTING EXPERIMENTS

The force controlled cutting experiment was carried out on an automatic cutting machine, designed to simulate the manual cutting process using abrasive discs, with a closed loop force control monitoring system. The normal force applied to the disc is pre-determined, as are the revolutions per minute. Once these values are set, the disc is attached to the machine, and the test begins. During the test, the machine remains closed until completion.



**Figure 13** - Schematic representation of the closed loop force control system.



Source: The author (2024).

The results of these tests include data on the mechanical forces (normal force and torque) acting on the disc, diametrical wear (which can be converted into the G-ratio), mechanical power required and speed. The test concludes either when the disc reaches the end of its life or when an error such as glazing or disc breakage occurs. Subsequently, the collected data is processed and analyzed.

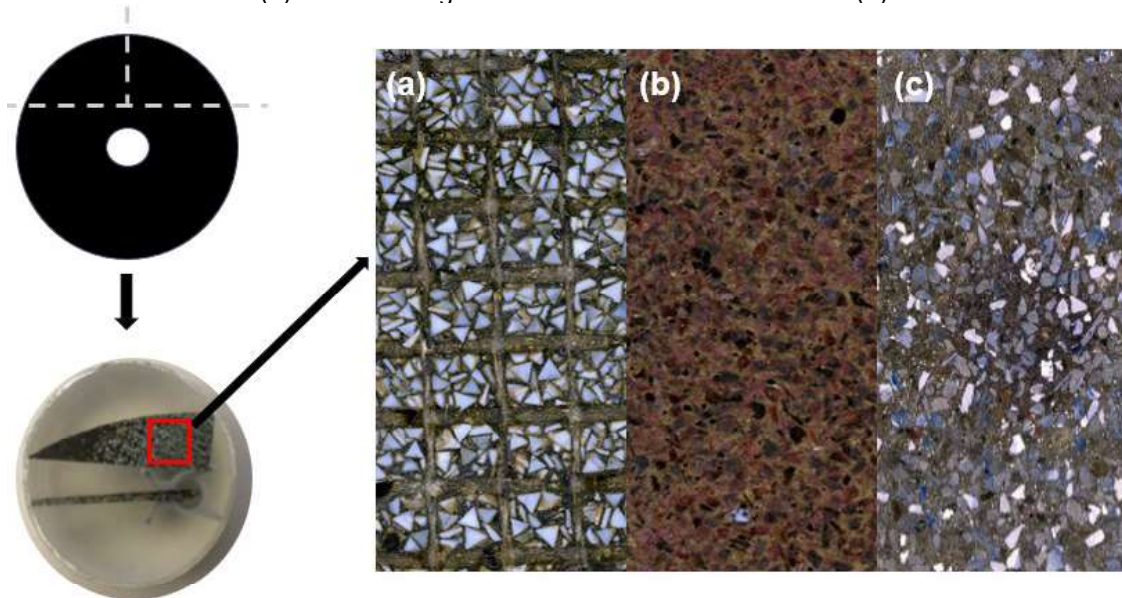
Three forces magnitudes and four distinct revolutions per minute were used: 40N at 7000 and 8000 rpm, 32N at 6500 rpm and 20N at 7000 rpm and 8000 rpm. The cutting material used was AISI 304 stainless steel.

## 4 RESULTS

### 4.1 TOOL CHARACTERIZATION

The microstructure of each disc was analyzed in an optical microscope. The images of each of the discs are disclosed in Figure 14.

**Figure 14** – Tool characterization by optical microscopy: Sol-gel aluminum oxide (a). Aluminum oxide (b). Zirconia toughened alumina and aluminum oxide (c).



Source: The author (2024).

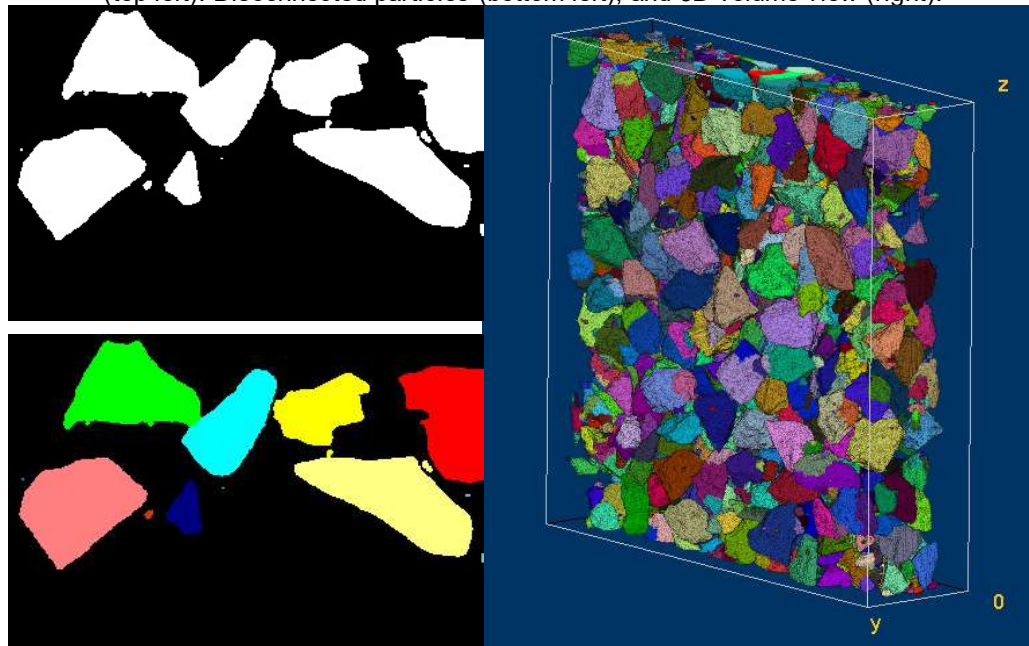
The abrasive grains in disc A appear as shaped triangles, byproduct of the meticulous control during the sol-gel process, as well as distributed in square section along the radial and width directions of the abrasive grit. In disc B, red corundum grains are discernible, suggesting the addition of  $\text{Cr}_2\text{O}_3$  to the grain to improve toughness. The distribution in this disc appears to be of irregular shape and form, but with stochastic distribution and similarly to the abrasives presented in disc C. As anticipated, disc C exhibits two distinct abrasive colors, reflecting the presence of two different abrasive types within the disc. Furthermore, it is observed that the abrasive grains of disc A, as well as having a triangular shape when viewed from the front, present a smaller thickness when viewed from the side. In contrast, discs B and C appear to have a more uniform geometry, with the same dimensions in all directions. Therefore, it can be stated that the number of abrasive grains in A, given a disc width

of 10 mm, could be higher. This is because, if the grains are all oriented in the same direction, they will take up less space.

#### 4.2 X-RAY COMPUTED TOMOGRAPHY (XCT)

The x-ray computed tomography, as previously mentioned, was conducted at a different laboratory, and only the resulting images were sent for evaluation. Images were processed using Fiji /ImageJ software, to facilitate the examination of the volume rate and distribution of particle sizes in the discs. Figure 15 provides an illustrative example of the image step-by-step guide utilized for the analysis of the samples. The volume rate is presented in the following Table 4.

**Figure 15** – X-ray computed tomography image analysis: identified abrasive grains with threshold tool (top left). Disconnected particles (bottom left), and 3D volume view (right).



Source: The author (2024).

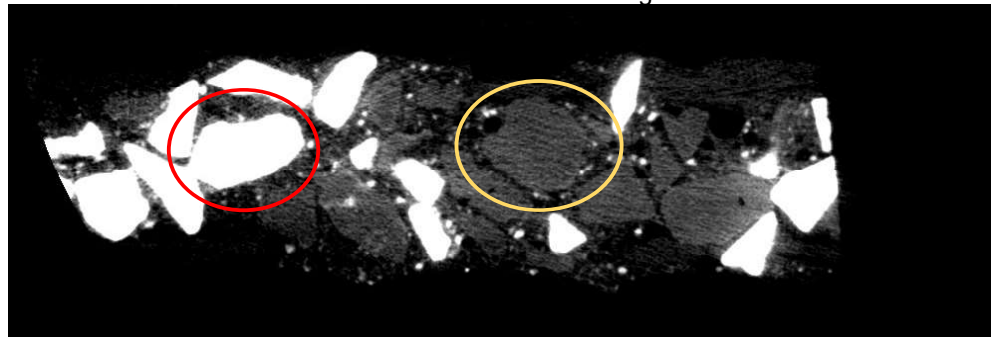
**Table 4** – X-ray computed tomography results: abrasive volume rate.

| Disc | Abrasive volume rate [%] |
|------|--------------------------|
| A    | 25.1                     |
| B    | 28.9                     |
| C    | inconclusive             |

Source: The author, 2024

It is known that disc C have a mixture of zirconium oxide and aluminum oxide as the abrasive materials. In Figure 16, we can identify the zirconia abrasive as the dark abrasive grains, indicated by the yellow circle, and the  $\text{Al}_2\text{O}_3$  abrasives as the white ones, indicated by the red circle.

**Figure 16** - XCT image of disc C. Red circle indicates aluminum oxide abrasive grains; yellow circle indicates zirconium oxide abrasive grains.



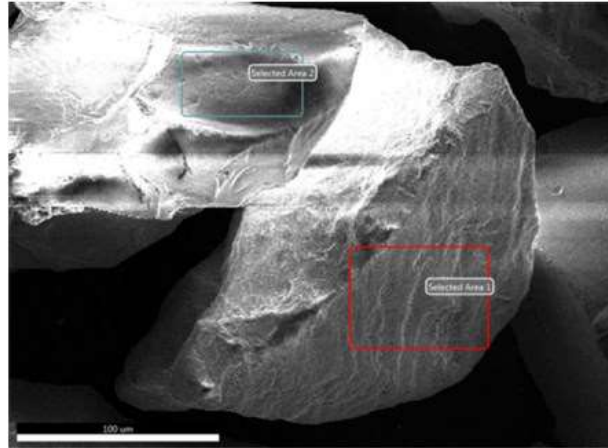
Source: The author (2024)

ImageJ software uses color contrast to identify different elements. In this case, the dark abrasive grains do not have enough contrast to make it possible to separate them from the color of the resin. Because of this, the volume ratio could not be calculated for disc C.

### 4.3 ASH ANALYSIS

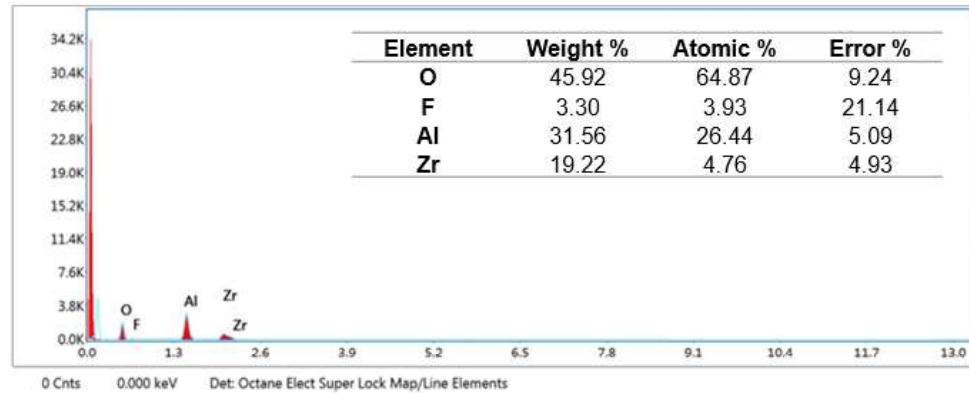
After the ash oven process, the abrasive grains, ashes, and fiber were analyzed separately. To determine the grain size, they underwent sieving through various pre-determined mesh sizes. The ashes were analyzed using Energy Dispersive X-ray Spectroscopy (EDX) to determine the chemical elements present and consequently, the type of filler and bond material used in each disc. To illustrate the results, the EDS spectrum analysis of disc C show the two different abrasive types to be analyzed (Figure 17) and the result specter of each abrasive (Figure 18 and Figure 19).

**Figure 17** – EDS analyzed areas of disc C



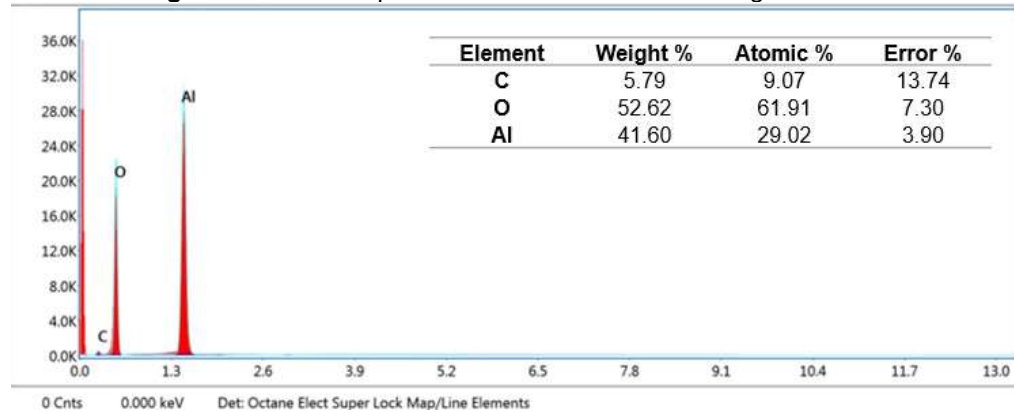
Source: The author (2024)

**Figure 18** – Result specter of area 1: ZTA abrasive grain



Source: The author (2024)

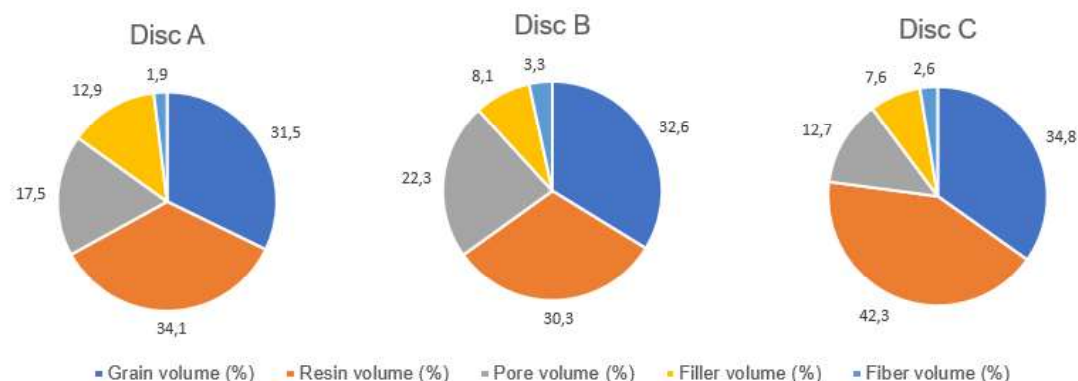
**Figure 19** – Result specter of area 2: Al<sub>2</sub>O<sub>3</sub> abrasive grain



Source: The author (2024)

The fiber was removed from the disc, and its dimensions were measured using a caliper. The volume composition of each disc and the identified filler and, fiber mesh size and abrasive grain size are shown in **Figure 20** and Table 5.

**Figure 20** – Volumetric composition of the discs.



Source: The author (2024).

**Table 5** – Ash analysis results.

| Disc | Abrasive grain type                               | Filler type    | Fiber [grams per meter square] | Grain size [mm] |
|------|---|----------------|--------------------------------|-----------------|
| A    | Sol-gel Al <sub>2</sub> O <sub>3</sub>            | PAF + cryolite | 60                             | 0.525 – 0.438   |
| B    | Al <sub>2</sub> O <sub>3</sub>                    | PAF            | 85                             | 0.438 – 0.370   |
| C    | ZrO <sub>2</sub> + Al <sub>2</sub> O <sub>3</sub> | Pyrite         | 85                             | 0.438 – 0.370   |

Source: The author (2024).

Comparing the results, it is evident that disc A exhibits a reduced grain volume in comparison to its counterparts; however, it compensates with larger grain sizes. Notably, disc A demonstrates a unique composition with two distinct fillers coexisting within the same disc, in contrast to discs B and C, each containing only one type of filler. Additionally, disc A features a smaller fiber size. Disc C presents a bigger volume of both grain and resin, when compared to the other two studied discs, and a significantly smaller volume of pores.

Primarily, the incorporation of sol-gel technology in the abrasive grain manufacturing process stands out as a crucial contributor to disc A's enhanced performance, aligning with the observations made by Klein (2013). Sol-gel technology affords precise control over various grain characteristics, including size, composition, and purity, thereby optimizing cutting efficiency and tool durability, as underscored by

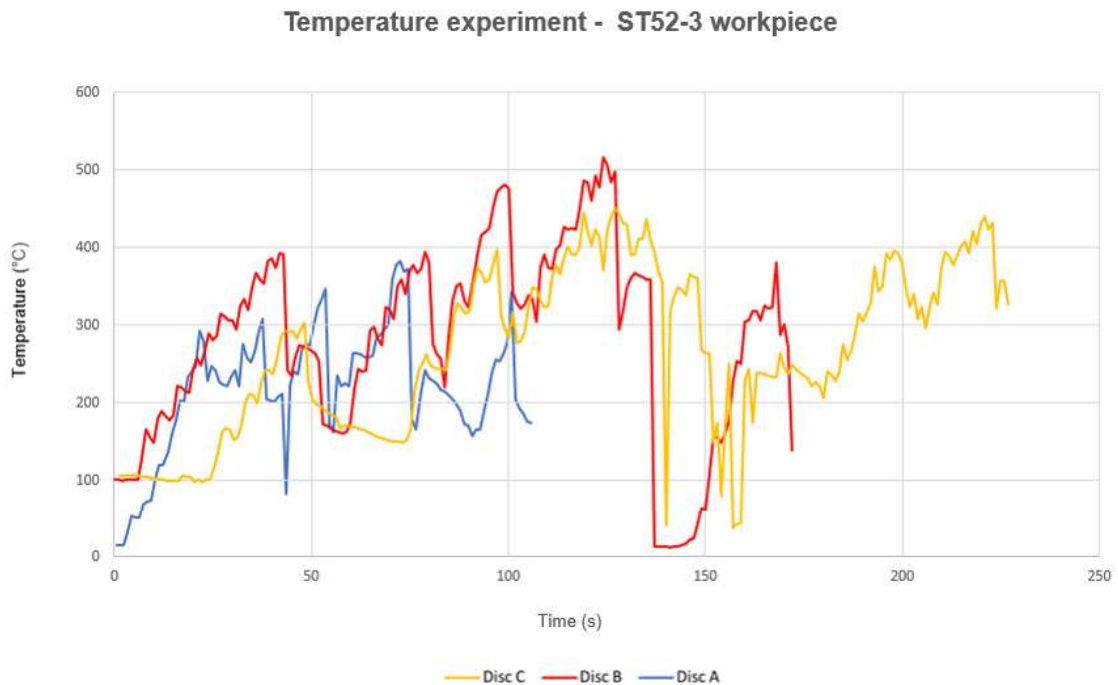


Starkov *et al.* (2014) and Naldony (2014). The microscopy and ash analysis revealing the triangular shape of the abrasive grains, along with their larger size and reduced volume per disc, further sets disc A apart from its competitors, echoing the importance of grain morphology highlighted in the literature.

#### 4.4 TEMPERATURE EXPERIMENTS

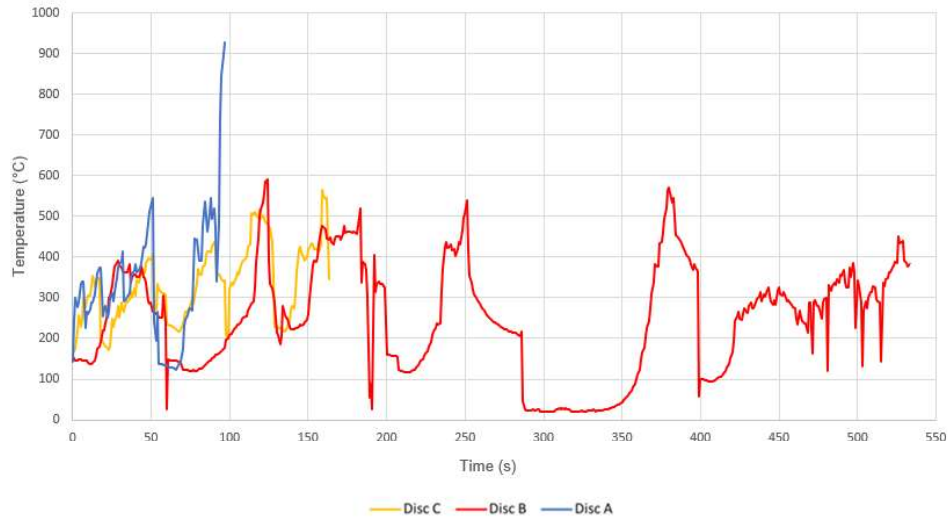
After removing moisture from the abrasive discs to ensure homogeneity, the cutoff experiments were carried out with a Hilti angle grinder AG 125-19SE handheld machine. In the Figure 21 and 22, are disclosed the temperature curve of all the experiments. The emissivity value used to set the infrared laser gun thermometer was  $\epsilon = 0,30$  for both workpiece steels. The workpieces were painted black to reduce the reflection.

**Figure 21** – Number of measurements vs temperature: stainless steel workpiece.



Source: The author (2024).

**Figure 22** – Number of measurements vs temperature: low carbon steel workpiece.  
 Temperature experiment - ST52-3 workpiece



Source: The author (2024).

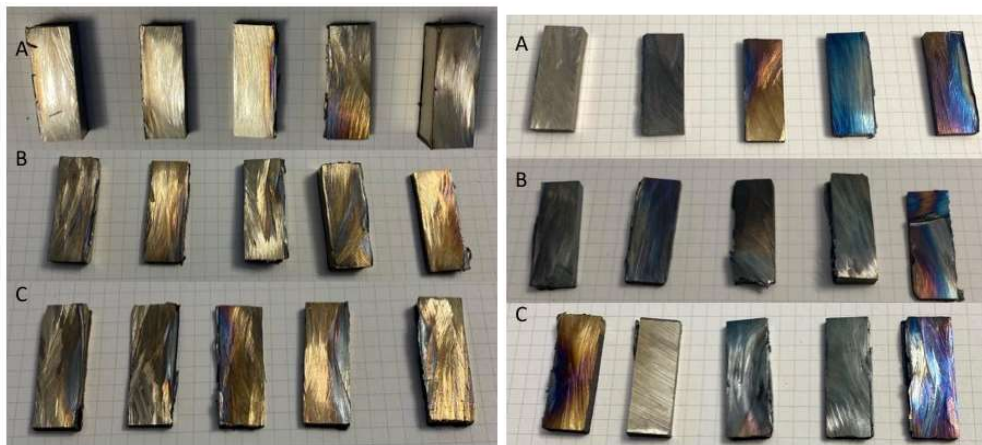
The graph fluctuates due to the manual cutting process, indicating the beginning and end of each cut. The peaks in the graph represent the end of each cut, signaling when the disc passes through the workpiece and the cutting process of one sample concludes. Five cuts are made per sample. It is important to note that the results depict the temperature of the workpiece during cutting, not the temperature of the cutting process itself. Hence, the temperature does not exceed 1000°C, as would be expected in abrasive cutting processes without lubrication.

As we can observe, cutting five samples using disc A was faster for both stainless steel, which required approximately 110 seconds, and low carbon steel, which took just under 100 seconds. When cutting the stainless steel workpiece, disc B was faster than disc C, approximately 175 and 275 seconds, respectively. However, for the low carbon steel sample, disc C cut faster, approximately 160 seconds, while disc B took 540 seconds.

Dry cutting using an abrasive disc can elevate the cut temperature beyond the tempering color. According to Ning, Rahman and Wong (2001), the higher the cutting speed and feed rate, the darker the color of the chip and the greater the degree of oxidation, which leads to a higher temperature. Consequently, it becomes feasible to identify the cutting temperature by examining the colors of both the sample extracted from the cut (Figure 23) and the produced chips (Figure 24).



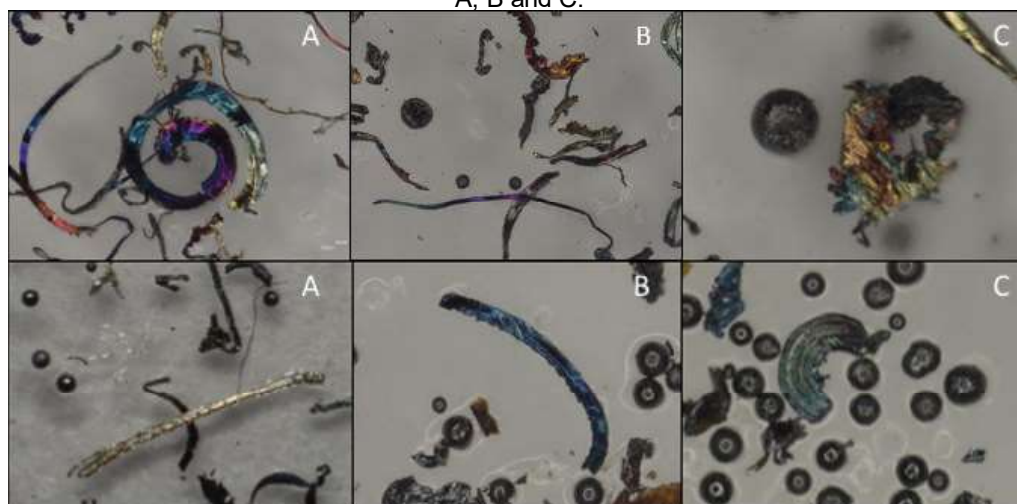
**Figure 23** – Sectioned workpieces of stainless (left) and low carbon steel (right). Disc A, B and C indicated in each row.



Source: The author (2024).

As expected, the stainless steel samples did not color as much as the low carbon steel ones, since they have chromium as an alloying agent, that mix with oxygen in the air to form a thin protective film on the surface of the metal and protect it from more visible corrosion. But even with the protective film, it is possible to identify some slight temper green, blue and golden colors in the samples cut with discs A, B and C. Indicating a cutting temperature ranging from 880 to above 1000°C.

**Figure 24** – Resulting chip morphology: low carbon (top), and stainless steel chips (bottom); for discs A, B and C.



Source: The author (2024).

Based on the Table 1 provided in the literature review chapter above, the chip hues can be correlated with the temperatures at which they were produced. As a result, one can predominantly notice green, blue, purple, and golden shades. Hence, it can

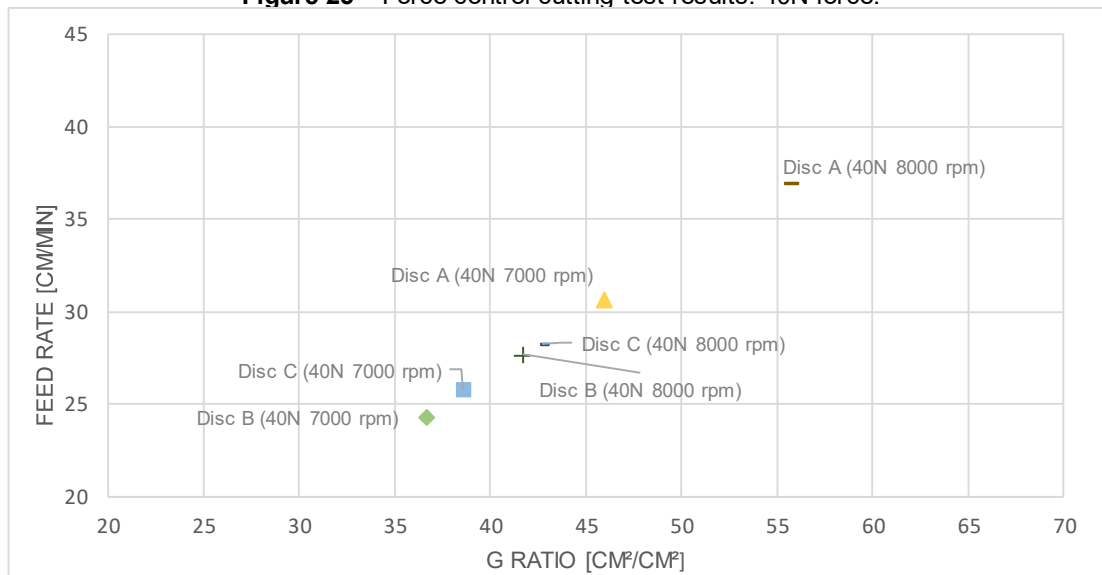
be concluded that the cutting temperature of the low carbon steel ST52-3 specimens using all three discs was consistent, varying between 880 to above 1000°C.

All cutting operations exhibited the formation of spherical chips, characterized by the generation of small spherical balls resulting from the interaction of the extremely hot chip with the surrounding air. The presence of numerous spherical chips suggests a high contact temperature exceeding the melting point of the workpiece material. Consequently, it can be theorized that the material of the chip undergoes a phase change, transitioning from a solid to a liquid state before solidifying once again. (KUFFA, 2017).

#### 4.5 FORCE CONTROL CUTTING EXPERIMENT

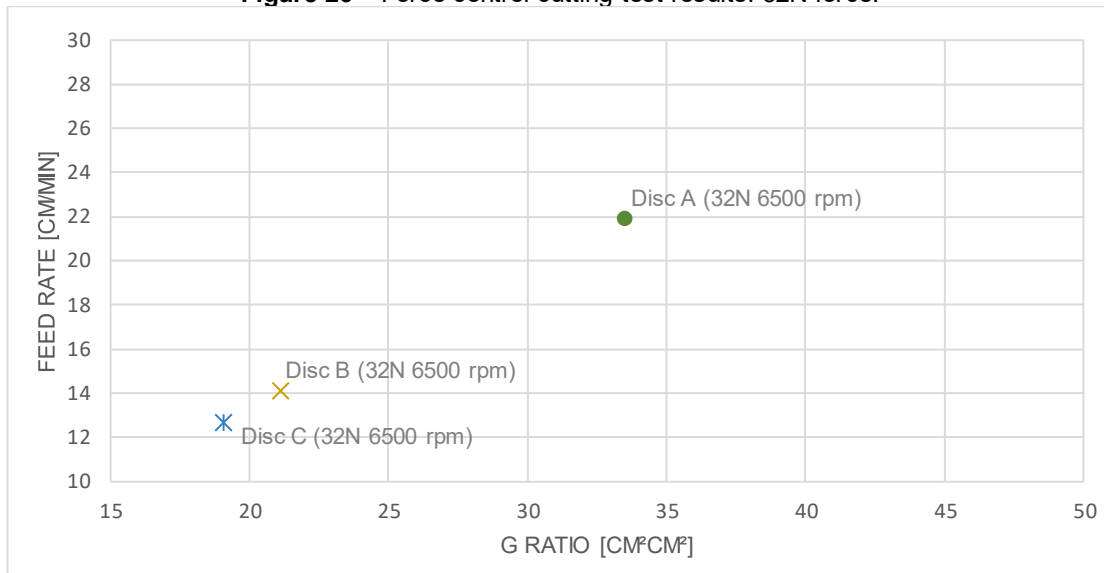
To compare the discs, the results of feed rate and grinding ratio were presented in graphs. The grinding ratio is determined based on the amount of wear on the workpiece, divided by the difference in diameter of the disc before and after the cutoff process, as measured by the automatic machine. The feed rate is calculated by dividing the disc width by the average time of cut. The results were categorized by variations in normal force, resulting in three separate graphs (Figure 26, Figure 27, and Figure 27, respectively). The optimal disc minimizes wear while maximizing feed rate.

**Figure 25** – Force control cutting test results: 40N force.



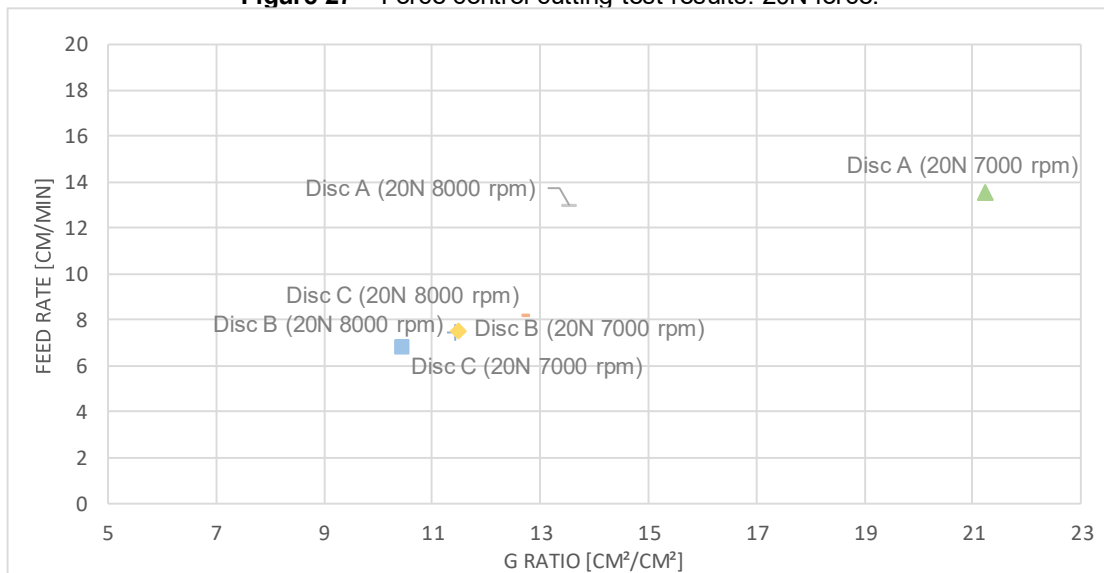
Source: The author (2024).

**Figure 26** – Force control cutting test results: 32N force.



Source: The author (2024).

**Figure 27** – Force control cutting test results: 20N force.



Source: The author, 2024.

It is consistently observable in all forces variations observable that disc A (Sol-gel Al<sub>2</sub>O<sub>3</sub>) exhibits the highest feed rate and grinding ratio. This finding aligns with existing literature. Linke (2016) reported that sol-gel corundum displayed notably lower radial wear and a higher maximum specific material removal rate compared to traditional corundum under conditions of high load or cutting speeds. The superior performance of sol-gel corundum can be attributed to its abrasive grains wearing

through micro-splintering, proving particularly effective at elevated cutting speeds and high material removal rates.

Disc C exhibits high feed speed and grinding ratio in tests with applied normal force of 40N, at both tested rotations per minute, 7000 and 8000rpm, as well as with a force of 20N and 8000rpm. However, in the test with 20N and 7000rpm, disc B shows higher feed speed, while disc C demonstrates a higher grinding ratio. This pattern repeats itself in the 32N test with 6500rpm.

As a result of these attributes, disc A demonstrates exceptional performance across multiple metrics. It exhibits a higher material removal rate and cutting speed, indicative of its efficiency in cutting tasks and potential for improved productivity. Additionally, disc A displays reduced tool wear and lower cutting forces, corroborating its resilience and efficacy in abrasive cutting procedures, as supported by Malkin (2008). Moreover, the speed in which the workpiece is sectioned is notably faster compared to its competitors, contributing to improved productivity. Additionally, disc A shows less tool wear and lower cutting forces, indicating its resilience and efficacy in abrasive cutting procedures, as illustrated in the force control cutting test results.

Nevertheless, it is important to acknowledge that the zirconia-based disc C offers greater durability compared to aluminum oxide discs B observed by Wang and Stevens (1989) is evidenced in this work by the force control test results. While aluminum oxide discs may wear out quicker, they offer faster cutting speeds, striking a balance between speed and longevity.

## 5 CONCLUSION

In conclusion, the outcomes from the experiments presented above, it is clear that disc A surpasses its counterparts in multiple aspects. The excellence of disc A can be credited to several key factors, as elucidated by both the findings of this study and insights from relevant literature, due to its exceptional performance in cutting speed, material removal rate, and tool durability. Despite the compromises involved, its overall efficiency and effectiveness establish it as an asset in industrial cutting activities.

The use of X-ray computed tomography (XCT) offered a notable advantage by allowing the geometry of the abrasive grain to be visualized in detail. The volumetric analysis provided by XCT proved to be more meaningful and informative than a two-dimensional (2D) analysis, offering a deeper understanding of the internal structure and distribution of the grains. Notably, disc A presented an important differentiator due to its triangular shape with a thin thickness, which directs the wear in a unique way. This shape, together with the uniformity between the grains, gives it distinct performance characteristics that are worth highlighting.

Furthermore, by examining the ash analysis of the discs and the results of the force control cutting experiment, it can be concluded that disc A, with its utilization of cryolite and potassium aluminum fluoride (PAF), benefits from both enhanced grinding effectiveness and prolonged durability, making it superior in terms of filler quality. Disc B, which also includes cryolite, offers enhanced performance but do not match the durability of disc A due to the absence of the PAF properties. On the other hand, disc C's use of pyrite focuses on durability, but its performance is not as optimized as disc A and B due to the absence of cryolite.

The most effective characterization technique in this study was the ash analysis. The results of this method provided critical information about the abrasive grain size, volume, and type. It enabled the identification of fillers and determined the volume of each element present in the discs. This detailed compositional data was instrumental in understanding the performance variations among the discs. Future research could focus on optimizing and modifying abrasive discs to further enhance the efficiency and effectiveness demonstrated by disc A. Additional studies should concentrate on the impact of specific additives, the resin bond, and other characteristics of the disc beyond the abrasive grains alone. Furthermore, investigations into improving grain distribution

could give valuable insights for developing discs with increased durability and higher material removal rates. The application of advanced monitoring techniques during cutting processes would also provide critical data for refining and enhancing cutting parameters.

## REFERENCES

- BHOWMIK, S. NAIK, R. Selection of abrasive materials for manufacturing grinding wheels. **Materials Today: Proceedings**. v. 5, n. 1, p. 2860–2864. Jan. 2018.
- BIANCHI, E.C. **Estudo do comportamento de discos abrasivos, em operação do tipo “cut-off” por mergulho basculante, submetidos a diversas condições de corte sem lubrificação**. Tese (Livre-docência). Faculdade de Engenharia e Tecnologia. Universidade Estadual Paulista, São Paulo. 1997
- BIANCHI, E.C; SILVA, E.J.; FRANÇA, T.V.; SILVA JUNIOR, C.E.; VALARELLI, I.D. Influência da dureza dos discos abrasivos no corte de materiais dúcteis. **Revista Matéria**. v.11, n.1, p. 24–29. 2006. Available at: doi:10.1590/s1517-70762006000100005.
- BORDIN, F.M.; MANTOVANI, I.F.; MOREIRA, A.D.; ARAUJO, L.M.; WEINGAERTNER, W.L.; FERNANDES, C.P. X-ray microtomography for conventional grinding wheel structure analysis. **The International Journal of Advanced Manufacturing Technology**, v. 113, 2021, pp. 2943-2950.
- CALLISTER JUNIOR, W. D. **Ciência e Engenharia de Materiais: uma introdução**. Rio de Janeiro: LTC - Livros Técnicos e Científicos Ltda, 2016.
- CARREIRA, L.A.S. **Avaliação da eficiência energética no processo de retificação de metal duro**. Orientador: Prof. Dr.-Ing. Carlos Eiji Hirata Ventura. 2022. Tese (Dissertação de Mestrado em Engenharia Mecânica) — Universidade Federal de São Carlos, São Paulo, 2022.
- COES L. Chemistry of Abrasive Action. Industrial and engineering Chemistry. **American Chemical Society**. V. 47, n.2, p. 2493 – 2494. Dec. 1955.
- COLLESELLI, K.; SCHWIEGER, K.H. Schleifscheiben und Schleifkörper. In: Becker/Braun. *Kunststoff-Handbuch 10-Duroplaste*, Hanser Verlag, Munich, p. 894–908, 1988.
- GOLDSTEIN, J. I., *et al.* **Scanning Electron Microscopy and X-ray Microanalysis**. New York: Springer, 2003
- GUIMARÃES, C. **Retificação plana de aços para moldes e matrizes em várias condições de corte e diferentes técnicas de aplicação de fluido de corte**. Orientador: Prof. Dr. Rosemar Batista da Silva. 2016. Tese (Doutorado em Engenharia Mecânica). Universidade Federal de Uberlândia, Minas Gerais, 2016.
- GUO, C.; MALKIN, S. Analysis of Transient Temperatures in Grinding. ASME. **Journal of Engineering for Industry**. V.117, n. 4, 571–577, Nov.1995. Available at: <https://doi.org/10.1115/1.2803535>.
- HABA Solutions in Plates. **Technical specification of Inox V2A stainless steel X5CrNi 18-10**. Material number 1.4301. Herrenberg, Germany. 2024.

HABA Solutions in Plates. **Technical specification of Kronstrukta52 engineering steel S355J2+N**. Material number 1.0577. Herrenberg, Germany. 2024

HOU, Z.B.; KOMANDURI, R. On the mechanics of the grinding process, Part III: Thermal analysis of the abrasive cut-off operation. **International Journal of Machine Tools & Manufacture**. V. 44, n. 2–3, p. 271-289, Set. 2004. Available at: <https://doi.org/10.1016/j.ijmachtools.2003.09.009>.

KLOCKE, F. **Manufacturing Processes 2: Grinding, Honing, Lapping**. Germany: Springer, 2009.

KNOP, A.; PILATO, L.A. **Abrasive Materials**. In: Phenolic Resins. Springer, Berlin, Heidelberg. 1985. Available at: [https://doi.org/10.1007/978-3-662-02429-4\\_17](https://doi.org/10.1007/978-3-662-02429-4_17)

KUFFA, M. **High Performance Dry Grinding: HPDG**. Supervisor: Prof. Dr.-Ing. Konrad Wegener. 2017. Thesis (Doctor of Sciences); ETH Zurich; 2017

LAZA, J. M. *et al.* Influence of Fillers on the Properties of a Phenolic Resin Cured in Acidic Medium. **Journal of Applied Polymer Science**. V. 108, p. 387–392. May. 2007. Spain. Available at: <https://doi.org/10.1002/app.26816>

LEIßNER, T.; DIENER, A.; LÖWER, E.; DITSCHERLEIN, R.; KRÜGER, K.; KWADE, A.; PEUKER, U.A. 3D ex-situ and in-situ X-ray CT process studies in particle technology: A perspective. **International Journal of Science and Technology of Powder and Particulate Materials**. V. 31, n. 1, p. 78-86. Oct. 2020. Available at: <https://doi.org/10.1016/j.apt.2019.09.038>

LINKE, B. **Life Cycle and Sustainability of Abrasive Tools**. Switzerland: Springer, 2016.

MACHADO, A.R.; ABRÃO, A.M.; COELHO, R.T.; da SILVA, M.B. **Teoria da Usinagem dos Materiais**. São Paulo: Editora Edgard Blucher, 2009

MALKIN, S. **The attritious and fracture wear of grinding wheels**. Supervisor: Prof. Nathan H. Cook. Thesis (Doctor of Sciences); Massachusetts Institute of Technology, 1968.

MALKIN, S.; GUO, C. **Grinding Technology: Theory and applications of machining with abrasives**. New York: **Industrial Press, Inc.** 2008

MARINESCU, I. D. *et al.* **Handbook of Machining with Grinding Wheels**. New York: CRC Press. 2007.

MARINESCU, I. D.; *et al.* **Handbook of Ceramic Grinding and Polishing**. Boston: Noyes Publishing, LLC. 2015



NADOLNY, K. State of the art in production, properties, and applications of the microcrystalline sintered corundum abrasive grains. **International Journal of Advanced Manufacturing Technology**, v. 74, p. 1445–1457, 2014.

NEUGEBAUER, R.; HESS, K.U.; GLEICH, S.; POP, S. Reducing tool wear in abrasive cutting. **International Journal of Machine Tools Manufacturing**. V. 45, n.10, p.1120–1123, 2005

NING, Y.; RAHMAN, M.; WONG, Y.S. Investigation of chip formation in high-speed end milling. **Journal of Materials Processing Technology**. V.113, n. 1–3, p. 360 – 367. 2001. Available at: [https://doi.org/10.1016/S0924-0136\(01\)00628-8](https://doi.org/10.1016/S0924-0136(01)00628-8).

ORTEGA, N.; MARTYNENKO, V.; PEREZ, D.; KRAHMER, D.M.; LACALLE, L.N.L.; UKAR, E. Abrasive Disc Performance in Dry-Cutting of Medium-Carbon Steel. **Metals**. V.10, n.4, p. 538. 2020. Available at: <https://doi.org/10.3390/met10040538>

RODRIGUES, A.G. **Caracterização do desgaste do rebolo na retificação de inserto de metal duro**. Orientador: Prof. Dr.-Ing. Carlos Eiji Hirata Ventura. Dissertação (Mestrado em Engenharia Mecânica); Universidade Federal de São Carlos. São Paulo. 2021.

RUDAWKSA, A. **Abrasive Technology: Characteristics and Applications**. Poland: InTech. 2018.

SAKKA, S. **Handbook of Sol-Gel Science and Technology**. Springer Science & Business Media.2005.

SHAW, M. C.; FARMER, D. A.; NAKAYAMA, K. Mechanics of the Abrasive Cutoff Operation. **ASME Journal of Engineering for Industry**. V. 89, n. 3, p. 495–502 Aug. 1967. Available at :<https://doi.org/10.1115/1.3610096>

STARKOV, V. K. ; RYABTSEV, S.A.; POLKANOV, E.G. ; KISKIN, O.S. Comparative Analysis of Performance of Cubic Boron Nitride and Microcrystalline Alumina Tools in Profile Grinding of Form Cutters. **Investigation of machining processes**. V. 36, n. 1, p. 43–48, 2014.

VENKATESH, V. C.; RYABTSEV, S.A.; POLKANOV, E.G.; KISKIN, O.S.A Study of Chip Surface Characteristics during the Machining of Steel. **CIRP Annals – Manufacturing Technology**. V. 42, n. 1, p. 631-636. 1993. Available at: [https://doi.org/10.1016/S0007-8506\(07\)62526-8](https://doi.org/10.1016/S0007-8506(07)62526-8).

VARASQUIM, F. **Otimização da retificação tangencial plana de compósitos plásticos reforçados com fibra de carbono**. Orientador: Prof. Dr. Eduardo Carlos Bianchi. Dissertação (Mestrado em Ciência e Tecnologia dos Materiais). Universidade Estadual Paulista. São Paulo. 2010

WANG, J.; STEVENS, R. Review: zirconia-toughened alumina (ZTA) ceramics. **Journal of Materials Science**. V. 24, p. 3421-3440. Set. 1989.

WEGENER K.; HOFFMEISTER, H.W.; KARPUSCHEWSKI, B.; KUSTER, F.;  
HAHMANN, W.C.; RABIEY, M. Conditioning and monitoring of grinding wheels. **CIRP  
Annals**. V. 60, n.2, p.757-77, 2011. Available at:  
<https://doi.org/10.1016/j.cirp.2011.05.003>

ZHANG, X. **Advances in Grinding and Abrasive Technology XVI**. Switzerland:  
Trans Tech Publications, 2013.